Nanomanufacturing and Metrology (2022) 5:283–296
https://doi.org/10.1007/s41871-022-00151-9

ORIGINAL ARTICLE

Isotropic Tuning of Electrochemical Etching for the Nanometric Finishing of Metals

Rong Yi[1] · Zejin Zhan[1] · Hui Deng[1]

Received: 22 May 2022 / Revised: 28 August 2022 / Accepted: 31 August 2022 / Published online: 20 September 2022

Abstract
Isotropic etching polishing (IEP) based on the merging of isotropic etch pits has been proposed as a generic metal finishing approach. In this work, the tuning of the etching isotropy of various metals, which is the key to realizing the finishing effect of IEP, is studied by theoretical analysis and etching experiments. The isotropic etching of various metals can be realized through mass transfer polarization by adjusting the electrochemical parameters. The addition of sulfuric acid in the electrolyte is the most effective for tuning the isotropy of electrochemical etching. It can decrease the diffusion coefficient of metal ions, thereby increasing the resistance of mass transfer and transforming the electrochemical dissolution of metal into mass transfer polarization. In this study, the atomic and close-to-atomic scale surface finishing of various metals and alloys has been successfully achieved through isotropic etching. After etching at a current of 1.5 A for 3 min, the surface Sa roughness of TA2 is drastically reduced from 242 to 3.98 nm. After etching for 1 min at a current of 3 A, the surface Sa roughness of pure tungsten, NiTi, and CoCrNi decreases from 9.33, 76.4, and 37.6 nm, respectively, to 1.16, 2.01, and 2.51 nm, respectively.

Keywords ACSM · Metal finishing · Isotropic etching polishing · Electrochemical polishing

1 Introduction

Surface finishing is essential for the application of metal components. Metal surface finishing can be efficiently realized by abrasion using hard abrasives [1–3]. However, scratches are inevitably formed during mechanical polishing [4], and ultrasmooth surfaces with nanometer-order roughness are rarely achieved [5]. Energy beam technologies, such as laser beams and electron beams, have been applied in the field of metal surface finishing to eliminate abrasion-induced damage [6, 7]. Energy beam polishing can achieve scratch-free and ultrasmooth metal surfaces and has been widely used for the finishing of 3D-printed metal parts. However, defects, such as surface oxidation, microcracks, and distortion, are inevitably introduced. This method is also limited by beam path interference [8]. Thus, lasers and electron beams are difficult to be used for the finishing of complex metal components without inducing surface property deterioration.

Compared with mechanical polishing and energy beam polishing, electrolyte-based polishing has the advantages of being abrasion-free, interference-free, and high efficiency [9, 10]. Electrochemical polishing (ECP) is a widely studied and utilized electrolytic polishing technique [9] based on the leveling effect of the viscous layer: given their small viscous layer thickness, the surface protruding sites have a high current density and are preferentially removed, eventually leading to a smooth surface [9]. ECP has been successfully applied for the surface finishing of several metals, such as tungsten and stainless steel [9, 11]. For metals and alloys with specific compositions, an appropriate electrolyte must be selected to form the viscous layer, which is not always realizable [9].

Compared with ECP, a more versatile electrolytic polishing technique named isotropic etching polishing (IEP) was proposed as a generic approach for metal finishing; IEP is based on the merging of isotropic electrochemical etching pits [12]. With this method, a lapped titanium surface was successfully polished to a mirror surface with the *S*a roughness reduced from 64.1 to 1.2 nm [12]. On the basis of the smoothing mechanism of IEP, the original rough surface is

✉ Hui Deng
dengh@sustech.edu.cn

[1] Department of Mechanical and Energy Engineering, Southern University of Science and Technology, No. 1088, Xueyuan Road, Shenzhen 518055, Guangdong, China

gradually replaced by the ultrasmooth inner surface of the isotropic etching pits, which eventually merge together and realize the whole surface polishing. Etching isotropy plays a key role in realizing the surface smoothing effect of IEP.

In this work, the mechanism and process to tune the etching isotropy of metals in electrochemical etching are proposed on the basis of mass transfer theory and charge transfer theory. The effects of electrolyte concentration, temperature, additives, and applied voltage on the etching isotropy of pure titanium are investigated. The oxidation film on the surface and the application of pulse supply power can also affect the etching isotropy by influencing the density of etching pits. Application results on pure nickel, stainless steel 304, and aluminum alloy 6063 demonstrate that etching isotropy can be controlled by adjusting the etching parameters. Furthermore, IEP is applied on shape memory alloy (NiTi), medium-entropy alloy (CoCrNi), and pure tungsten. The acquired smooth surface shows that the control of etching isotropy during metal dissolution is an effective approach for metal polishing.

2 Electrochemical Etching of Metals

The electrochemical dissolution of metallic materials on the surface consists of two tandem processes: charge transfer and mass transfer [13, 14]. As shown in Eq. (1), charge transfer, also known as the electrochemical step, refers to the metal atoms losing electrons and becoming metal ions. Mass transfer refers to the reaction products, such as metal ions, diffusing from the surface toward the bulk solution, as shown in Eq. (2). These steps are in a series; hence, the process with great resistance and slow reaction rate is called the rate-determining step, which determines the final rate and dissolution characteristic of the dissolution reaction.

$$M - ne \rightarrow M^{n+} \tag{1}$$

$$M^{n+}_{\text{ads}} \rightarrow M^{n+}_{\text{bulk}} \tag{2}$$

2.1 Charge Transfer

For charge transfer, the metal needs to overcome its chemical activation energy and the electric field between the electrode surface and solution. According to transition state theory [15], when the electric field U is applied to the metal, the current density can be expressed as:

$$i = i_0 \times \exp\left(\frac{\alpha nF\left(U - \frac{\Phi+\Delta\Phi}{e}\right)}{RT}\right) = c_M nF\frac{kT}{h}\exp\left(\frac{\alpha nFU - \Delta G_0}{RT}\right) \times \exp\left(\frac{E_{\text{surf}}}{\rho kT}\right) \tag{3}$$

where c_M is the concentration of the metal atom of the surface; n is the number of electrons in the reaction; F, k, T, h, and R are the Faraday constant, Boltzmann constant, absolute temperature, Planck constant, and gas constant, respectively; α is transfer coefficient; ΔG_0 is the partial activation energy and is only related to the material; E_{surf} is the surface energy; and $\rho = N/S$ is the surface atomic density.

According to Eq. (3), the dissolution rate of the metal surface is determined by the temperature, the concentration of the metal atom on the surface, the applied potential, and the surface energy. For different crystal surfaces, the dissolution rates vary due to their differences in atom concentration and surface energy [16–18]. Therefore, when charge transfer is the rate-determining step, the dissolution of the metal is supposed to be anisotropic [19, 20].

2.2 Mass Transfer

In an unstirred or stagnant solution with no density gradients, the mass transfer in solution occurs by diffusion and migration, which are the results of a gradient in electrochemical potential. According to the linear mass transfer formula [21], the current density at any location in solution during electrolysis is composed of contributions from all species and can be expressed as:

$$i = \frac{F^2}{RT} \times \frac{\partial\phi}{\partial x}\sum_j z_j^2 D_j C_j + F\sum_j z_j D_j \frac{\partial C_j}{\partial x} \tag{4}$$

where F, R, T, $\frac{\partial\phi}{\partial x}$, and x are the Faraday constant, gas constant, absolute temperature, potential gradient, and distance from the electrode, respectively; and z_j, D_j, and C_j are the charge, diffusion coefficient, and concentration of species j, respectively.

According to Eq. (4), for a particular system, the mass transfer current density is controlled by the temperature, potential gradient, and diffusion coefficient. Different from charge transfer, mass transfer is independent of the surface crystalline orientation. Hence, when the mass transfer is the rate-determining step, the dissolution of the metal is supposed to be isotropic [22, 23].

2.3 Tuning of Etching Isotropy

On the basis of the theoretical analysis of metal dissolution, the etching isotropy can be tuned by optimizing the etching parameters, and isotropic etching can be realized under mass transfer polarization conditions. Figure 1a and b shows the

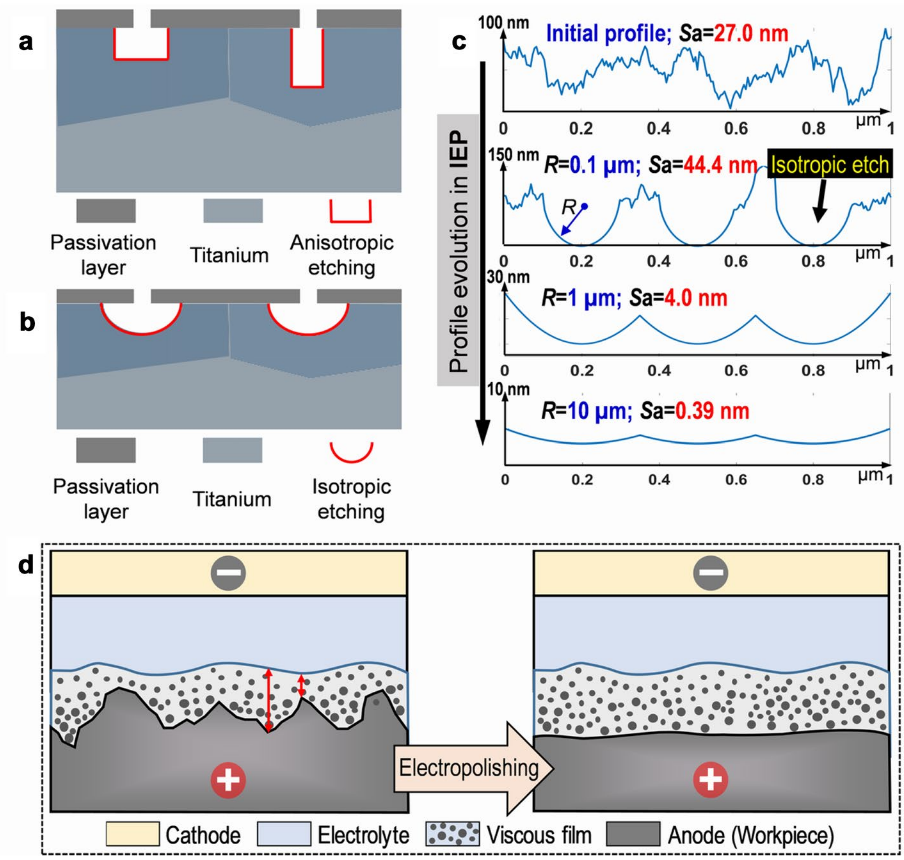

Fig. 1 **a** Image of anisotropic etching and **b** isotropic etching. **c** Simulation of the surface profile and roughness evolution during isotropic etching polishing and **d** schematic of the mechanism of electropolishing

images of anisotropic and isotropic etching. In the electrochemical process, the metal surface is always passivated first, and an oxide film is then formed [24]. Some weak sites of the passivation layer are preferentially broken down, and the dissolution of bulk material starts beneath the breakdown sites. If the etching process is anisotropic, as shown in Fig. 1a, then different planes have different etching rates, and the surface is impossible to smoothen. However, if the etching process is isotropic regardless of the grain orientation, then the gradual growth and merging of the etching sites will make the surface smooth. This phenomenon is the principle of IEP.

Figure 1c illustrates a rough surface gradually smoothened by IEP. The evolution of the surface profile and roughness during IEP was simulated using MATLAB. First, the initial rough surface was simulated using the fast Fourier transform method. A 1D matrix was randomly generated, with the matrix size set as the number of pixels in one surface measurement. Fourier transform was then performed on the random matrix, and the result was multiplied by an autocorrelation function that describes the degree of correlation between data at different locations. Finally, an inverse Fourier transform was conducted on the product to obtain the convex height of the original simulated rough surface. The autocorrelation function was expressed in an exponential form as follows:

$$H = \sigma^2 \exp(-\frac{\tau}{\beta}) \tag{5}$$

where σ represents the standard deviation, τ represents the sampling interval, and β represents the autocorrelation length.

The etching holes are semicircle and randomly distributed, so the expression of the height of the etching hole can be given as:

$$h = \sum_{1}^{n} \left[y_k - \sqrt{R^2 - (x - x_k)^2} \right] \tag{6}$$

where x_k, y_k refers to the random spatial position of the etching hole, and R refers to the radius of the semicircle holes.

By combining Eqs. (5) and (6), we obtained a surface height expression that represents a random rough surface with semicircle polished holes. Different stages of IEP can be simulated by adjusting the size of the semicircle holes.

A rough surface is smoothened due to the formation and merging of randomly distributed and continuously growing isotropic etch pits. On rough surfaces, isotropic etching occurs randomly, and the roughness first increases due to the generation of etch pits. However, the roughness rapidly decreases once the etch sites merge together. Eventually, an ultrasmooth surface with extremely low roughness is obtained when the radius of the etch pits is large enough. Figure 1d illustrates the mechanism of electropolishing for comparison with that of IEP. Both processes are electrolytic with similar polishing setups. Electropolishing is based on the leveling effect of nonuniformly distributed viscous films. Here etching isotropy plays a key role in IEP; thus, the mechanism of isotropy tuning must be elucidated for the further development of IEP.

Equations (3) and (4) show that the temperature, applied voltage, and diffusion coefficient are important factors affecting etching isotropy. Owing to the interaction between different parameters, the coordination of various parameters is crucial. In the following experiments, the effects of different etching parameters on etching isotropy were studied.

3 Experimental Approach

Figure 2 provides a schematic of the IEP setup. Commercially available pure titanium (TA2), pure nickel, stainless steel (304), aluminum alloy (6063), and tungsten substrates with a diameter of 15 mm and thickness of 3 mm were used in this study. The substrate was selected as the anode and connected to the positive electrode of the DC power (Keysight E3649A). Only the surface toward the cathode (platinum sheet: 2 cm × 2 cm) was etched or polished. Before etching, the substrates were lapped with SiC sandpapers (#500) to remove the rough cutting marks formed by wire cutting and then cleaned with deionized water and ethyl alcohol to remove contaminants. The distance between the cathode and anode was maintained at 60 mm. A mixed solution of analytical-grade sulfuric acid (H_2SO_4, 97%) and methanol (CH_3OH, 99.5%) was used as the electrolyte.

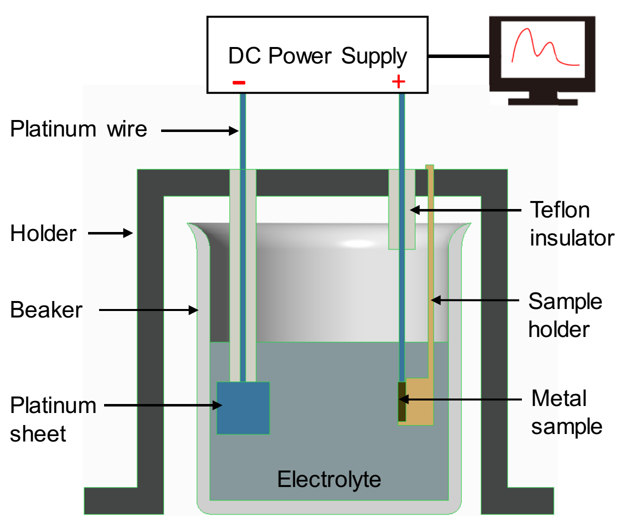

Fig. 2 Schematic representation of the experimental setup of electrochemical etching

The surface morphology of the etch sites was observed by scanning electron microscopy (SEM, ZEISS Merlin and Hitachi TM4000Plus). The thickness of the passivation layer was confirmed using transmission electron microscopy (TEM, JEM 3200FS). The surface roughness was measured by scanning white light interferometer (SWLI, Taylor Hobson, CCI) and atomic force microscopy (AFM, Bruker Edge). All electrochemical tests were carried out on an electrochemical workstation (CHI660E, Chen Hua instrument) using a three-electrode electrochemical system. The conductivity was measured by a conductivity meter (Mettler Toledo, INLAB 731-ISM).

4 Results and Discussion

4.1 Electrolyte Selection

The electrolyte is the carrier of current and reaction products, and its composition is an important factor affecting the dissolution rate and surface quality of metals [25]. Hence, the electrolyte composition for the etching of pure titanium (TA2) was first selected. Considering that titanium is more likely to form an oxide film rather than dissolve in an aqueous solution, methanol was selected as the basic electrolyte [26, 27]. The effect of different additives [28], such as sodium chloride (1 g/100 ml), and sodium hydroxide (1 g/100 ml), on etching morphology was also studied. For preliminary investigation, the polarization curves of pure titanium in different electrolytes were measured. As shown in the polarization curve of pure titanium in electrolyte with only methanol in Fig. 3a, the current increased sharply when the voltage exceeded 0.15 V (vs. Ag/AgCl), indicating the breakdown of the passivation layer [29, 30]. A similar result was also observed on the polarization curve of pure titanium in electrolytes with methanol and sodium chloride. As shown in Fig. 3b, the current increased when the voltage exceeded − 0.1 V (vs. Ag/AgCl), indicating the breakdown of the passivation layer. However, in the electrolyte with methanol and sodium hydroxide, the current increased slowly when the voltage exceeded 1.5 V (vs. Hg/HgO), as shown in Fig. 3c, corresponding to the formation of oxide film on the surface [31].

According to the results of the polarization curve, pitting occurred on the pure titanium in the electrolyte consisting of methanol or methanol and sodium chloride when the voltage exceeded a certain value [32]. The pure titanium substrates were etched in different electrolytes for 1 min at room temperature, and the current and voltage of the DC power supply were set at 0.02 A and 30 V, respectively. As shown in Fig. 3d, the TA2 substrate was etched in methanol

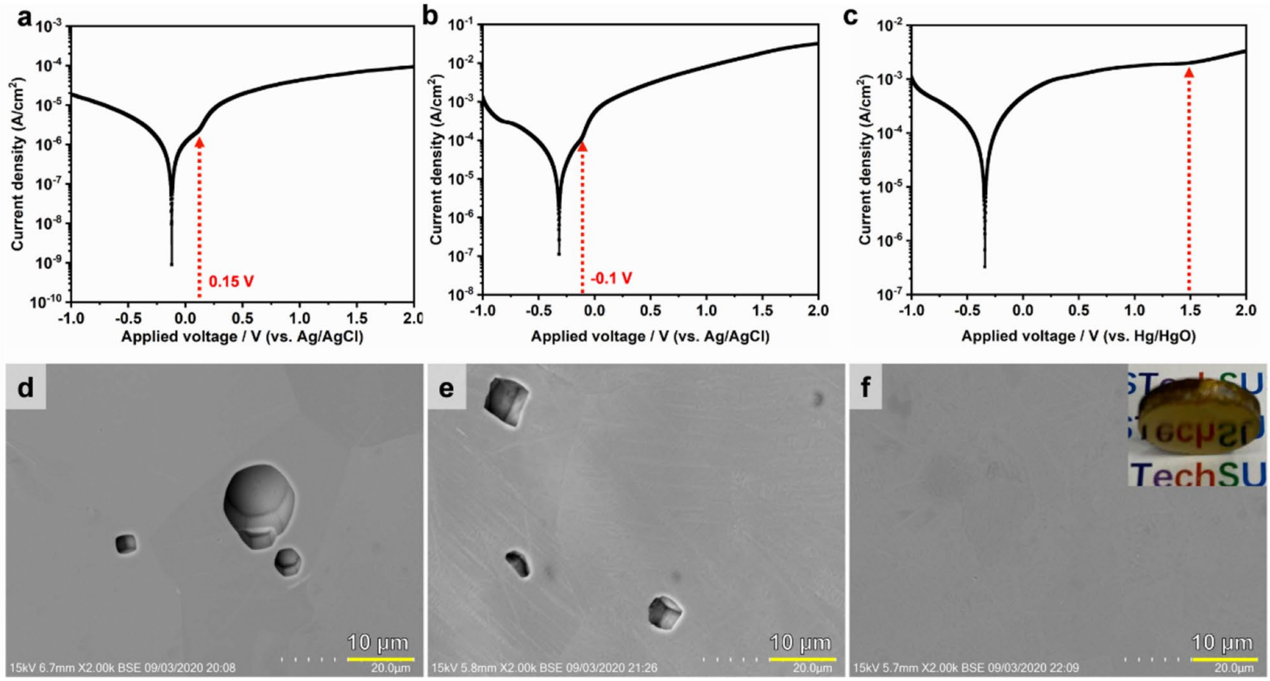

Fig. 3 Polarization curve and surface morphology of TA2 in the electrolyte composed of **a**, **d** methanol, **b**, **e** methanol and sodium chloride, and **c**, **f** methanol and sodium hydroxide

without any additives, and anisotropic etching pits with different shapes were formed on the surface due to the difference in the surface energy of different crystal surfaces [33]. Some etching pits were connected to each other, resulting in complex-shaped etching pits. During etching, the current was only 0.5 mA, which was far below the set value of 0.02 A even after the voltage reached 30 V. Given that the conductivity of methanol is only 1.5×10^{-9} S/m, the voltage drop was mainly consumed by the electrolyte. Therefore, solution conductivity must be increased by adding the appropriate additives.

As shown in Fig. 3e, the TA2 substrate was etched in methanol with 1 g/100 ml sodium chloride. Anisotropic etching pits were also formed on the surface, indicating that charge transfer is the rate-determining step [34]. The addition of sodium chloride increased the conductivity of the electrolyte to 0.838 S/m. However, the shape of the pits was irregular, indicating that the dissolution rate of different crystal surfaces of the metal was unstable.

As shown in Fig. 3f, the TA2 substrate was etched in methanol with 1 g/100 ml sodium hydroxide, and the conductivity of the electrolyte was 1.365 S/m. After etching, no etching pits were observed on the surface. As shown in the insert of Fig. 3f, a dark yellow oxide film was formed on the surface, indicating that the sodium hydroxide in the electrolyte promoted the formation of titanium oxides [29] and prevented the generation of etching pits. This result is consistent with the polarization curve.

On the basis of the discussion above, different additives increased the conductivity of the base electrolyte. However, the etching in electrolytes containing sodium chloride was unstable, and sodium hydroxide promoted the formation of an oxide film on the surface. Therefore, in the following experiment, the effect of sulfuric acid with high viscosity on the etching isotropy of pure titanium was investigated.

4.2 Etching Isotropy

In the theoretical analysis of the metal dissolution process, it is considered that the etching anisotropy and isotropy can be tuned by optimizing the etching parameters and isotropic etching can be realized under mass transfer polarization conditions. One approach is to increase the concentration of H_2SO_4 in the electrolyte. Given that the viscosity of H_2SO_4 (20.2 mPa·s at 25 °C) is higher than that of CH_3OH (0.55 mPa·s at 25 °C), the high concentration of H_2SO_4 increased the viscosity of the electrolyte and suppressed the diffusion of dissolved metal ions from the metal surface to the bulk solution [27]. Thus, mass transfer became the rate-determining step, and isotropic etching can be realized.

The linear sweep voltammetry (LSV) curves of pure titanium in two electrolytes are shown in Fig. 4a. In the electrolyte with a 1:100 volume ratio of H_2SO_4:CH_3OH, the measured LSV curve consisted of an active region, an extremely short passive region, and a transpassive region

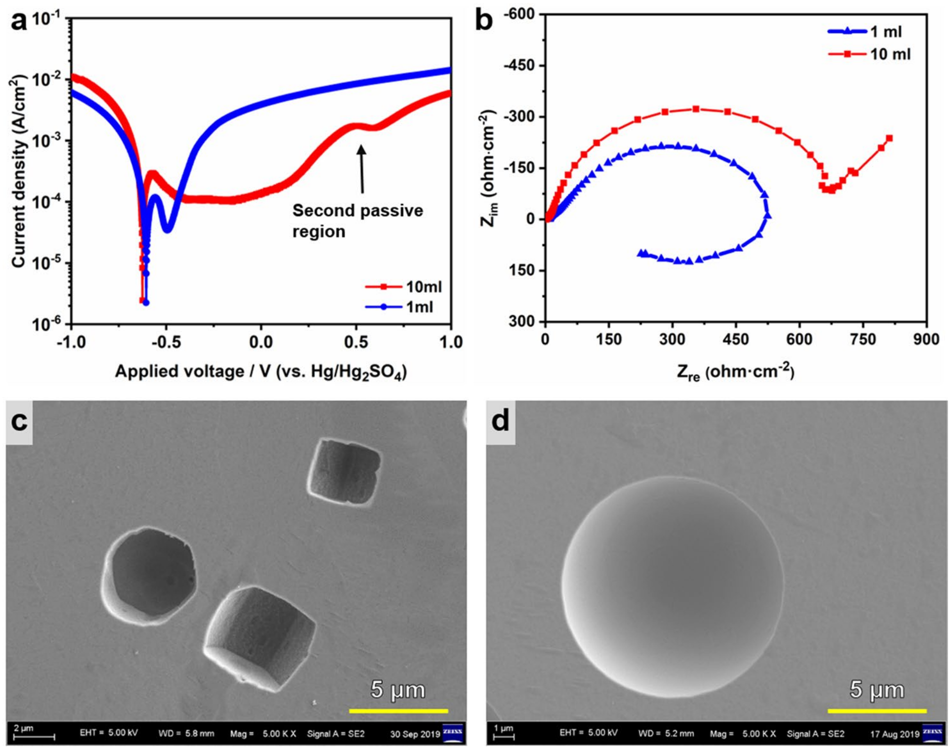

Fig. 4 **a** Polarization curves and **b** EIS plot in electrolyte composed of different concentrations of sulfuric acid, **c** SEM image of anisotropic etch pits of TA2 in electrolytes with a 1:100 vol. ratio of H_2SO_4 to CH_3OH, and **d** SEM image of isotropic etch pit of TA2 in electrolytes with a 10:100 vol ratio of H_2SO_4 to CH_3OH

[35, 36]. When the voltage was increased to − 0.5 V (vs. Hg/Hg_2SO_4), the passivation of anodic polarization was interrupted by a sharp increase in current, indicating the initiation of pitting corrosion [37]. In the electrolyte with a 10:100 volume ratio of H_2SO_4:CH_3OH, the LSV curve showed a different phenomenon: secondary passivation [38] occurred at a voltage of 0.5 V (vs. Hg/Hg_2SO_4). A possible explanation is that the strong oxidation of H_2SO_4 repaired the breakdown sites formed by the first transpassivation and then reduced the dissolution rate of the matrix [35, 38]. When the voltage exceeded 0.65 V (vs. Hg/Hg_2SO_4), the current increased again, indicating that the titanium began to dissolve. The passivation region of the polarization curve measured in the electrolyte with a 10:100 volume ratio of H_2SO_4:CH_3OH was from − 0.45 to 0.2 V (vs. Hg/Hg_2SO_4), which was larger than that measured in the electrolyte with 1:100 volume ratio of H_2SO_4:CH_3OH. This finding indicated that the high concentration of sulfuric acid improved the pitting resistance of TA2 [37, 39].

The electrochemical impedance spectroscopy (EIS) of pure titanium in two electrolytes is shown in Fig. 4b. A capacitive loop was found in the high-frequency range, and an inductive loop was observed in the low-frequency range in the Nyquist plot obtained in the electrolyte with a 1:100 volume ratio of H_2SO_4:CH_3OH. The capacitive loop indicated Faradaic charge transfer behavior, and the inductive loop indicated pitting corrosion [30]. The EIS spectrum indicated that the dissolution was kinetically controlled, and charge transfer was the rate-determining step in low frequency. However, for the Nyquist plot obtained in the electrolyte with a 10:100 volume ratio of H_2SO_4:CH_3OH, the capacitive loop occurred in the high-frequency range. A Warburg impedance, which represents the linear diffusion of charged species [40], occurred in the low-frequency range, demonstrating that the dissolution at low frequency was controlled by mass transfer.

TA2 substrates were etched with a constant current of 0.02 A for 1 min in two electrolytes with 1:100 and 10:100 volume ratios of H_2SO_4:CH_3OH. Figure 4c and d shows that with the increasing volume ratio, the morphology of the etch pits transformed from a polyhedral structure to a regular hemispheric structure, demonstrating the tuning of anisotropic etching to isotropic etching. This transformation revealed that increasing the viscosity of the electrolyte is a feasible method for tuning the etching isotropy due to mass transfer being slowed down in the electrolyte with high viscosity and becoming the rate-determining step.

4.3 Breakdown of the Passivation Layer

The excellent corrosion resistance of titanium is mainly due to the spontaneous formation of a passive film on the surface [41]. As shown in Fig. 5a, the thickness of the passivation layer was measured by TEM. A thin layer of 12 nm was formed on TA2. The weak sites of the passivation layer were preferentially broken down by the strong electric field. Figure 5b shows the SEM image of the broken passivation layer. Electrochemical etching took place at the breakdown

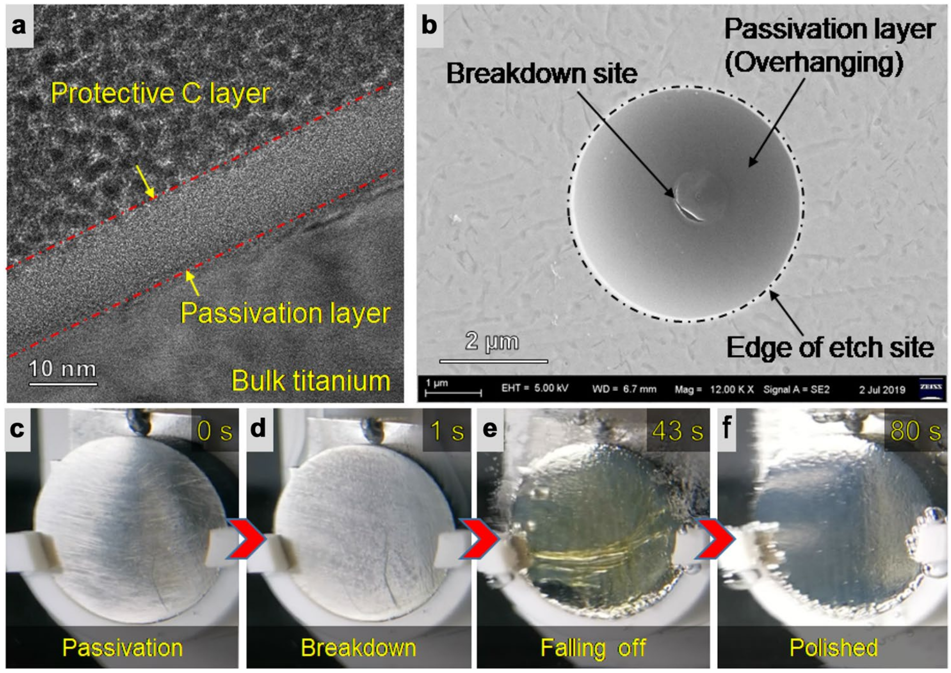

Fig. 5 **a** Cross-sectional view of the passivation layer on TA2 observed by TEM. **b** SEM image of a breakdown and etch site. **c**–**f** Photos of the sample surface during electrochemical etching at different durations

sites, and the material beneath the breakdown sites was dissolved. Thus, etch pits were formed beneath the passivation layer. The hemispherical shape of the etch pits indicated isotropic etching. The hemispherical etch pits were enlarged, overlapped, and eventually merged together (only the neighboring pits). As a result, the passivation layer dislodged, and the initially rough surface was eventually replaced by the smooth etched surface of the merged isotropic etch pits.

Figure 5c–f shows the sequential images of electrochemical etching. The passivation layer on the TA2 substrate surface was broken down after a short duration. Lapping marks were no longer observed after etching pits formed at the breakdown sites. After the etch pits grew, the passivation layer detached (Fig. 5e) and a refreshed and smooth surface was formed, as shown in Fig. 5f.

4.4 Tuning of the Etching Isotropy of Titanium

According to Eqs. (3) and (4), etching anisotropy and isotropy can also be affected by other parameters, such as temperature and potential (Fig. 6). Temperature can affect charge transfer and mass transfer. As shown in Figs. 6a1–a3, anisotropic etch pits were formed when the temperature was 10 °C or 30 °C. However, isotropic etch pits were formed at a medium temperature of 20 °C. As described in Eqs. (3) and (4), the effect of temperature on charge transfer and mass transfer is complicated; therefore, precisely determining the rate-determining step during temperature increase is difficult. Similarly, the effect of potential was investigated. Potential showed an exponential effect on the charge transfer and a linear effect on the mass transfer. Meanwhile, charge transfer polarization can only occur when the potential is small. Thus, mass transfer polarization can be achieved by increasing the potential. Increasing the etching potential also increased the density of breakdown sites. According to the morphology of the etching pits shown in Fig. 5b, the mass transfer cross-sectional area was the size of the breakdown area, which was smaller than the whole inner surface of the etching pit where electron transfer occurred. Therefore, increasing the etching sites has a great promoting effect on mass transport. Finally, an excessive increase in potential will cause the electron transfer to be the rate-determining step. Figure 6b1 shows that when the potential was 0.5 V, anisotropic etching pits formed on the substrate and the density of etching pits was low due to the relatively low potential. When the potential was increased to 2 V, isotropic etching pits were formed on the surface due to the electron transfer rate rapidly increasing with the voltage, as shown in Fig. 6b2. However, when the potential was increased to 4 V, the etching was anisotropic due to the increase in etching pit density, as shown in Fig. 6b3.

A simple method for tuning the etching anisotropy is the addition of glycerine ($C_3H_8O_3$), which has a high viscosity. Figure 6c1–c3 shows that after adding 5 ml of $C_3H_8O_3$ to the electrolyte, the etching was still anisotropic. This result was the same as that obtained without $C_3H_8O_3$ addition. However, hemispheric isotropic etch pits were formed when 10 ml of $C_3H_8O_3$ was added to the electrolyte. Therefore, adding a certain amount of high-viscosity $C_3H_8O_3$ can convert the etching anisotropy to isotropy by reducing the diffusion rate of ions and making mass transfer the

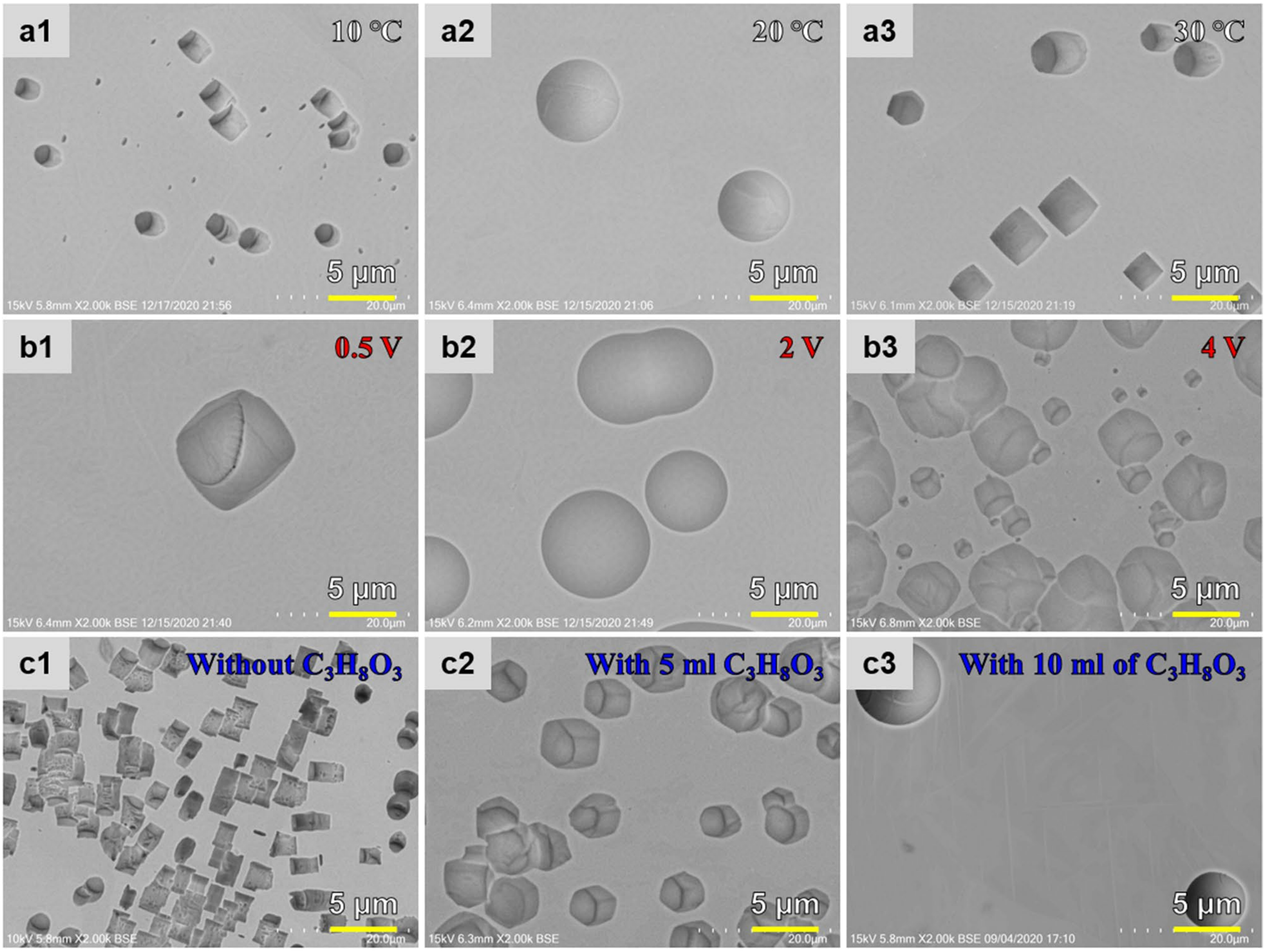

Fig. 6 Tuning the etching isotropy of TA2 by different parameters. **a1**–**a3**: etch pits formed under different temperatures (0.02 A, 1 min, H_2SO_4:CH_3OH = 4:100); **b1**–**b3** etch pits formed by different potentials (20 °C, 2 min, H_2SO_4:CH_3OH = 4:100); **c1**–**c3** etch pits formed with different concentrations of $C_3H_8O_3$ (20 °C, 0.02 A, 1 min, H_2SO_4:CH_3OH = 1:100)

rate-determining step for metal dissolution. In addition, etching efficiency decreases when a highly viscous electrolyte is used.

In addition to the parameters indicated in Eqs. (3) and (4), the surface state affects etching isotropy. The procedure of sample preparation is shown in Fig. 7a. Two TA2 substrates were etched with a constant current of 0.1 A for 1 min in electrolyte with a 1:100 volume ratio of H_2SO_4:CH_3OH, and sample b was previously anodically oxidized in 1 wt% NaOH solution for 10 s with an applied voltage of 15 V. As shown in Fig. 7b, the thickness of the oxide film formed on sample b was about 20 nm. As shown in Fig. 7c, anisotropic etching occurred due to the low concentration of sulfuric acid, and the anisotropic etching holes bound to each other due to the relatively high current. However, isotropic etching occurred on the surface that was previously anodically oxidized, as shown in Fig. 7d. Compared with the passivation film formed spontaneously, the anode oxide film was thicker and more difficult to be broken down. Thus, only a few etching sites were formed on the anodized surface. Few etching sites mean few mass transfer channels. Given that the constant current mode was adopted, the amount of mass transferred was the same. Thus, the concentration of dissolved metal ions was high around the etching sites on the anodized surface. Therefore, the mass transport rate was relatively reduced, resulting in mass transport becoming the rate-determining step and the etching becoming isotropic.

Another way to increase the density of the etching site is to use a pulse power supply. After each pulse, the passivation film will re-form on the surface, and breakdown will occur again on the surface when the next pulse is in progress [42]. Therefore, increasing the pulse frequency can increase the number of breakdowns and consequently the number of etching sites. In this research, a unipolar square wave power supply with a duty cycle of 50% was used. The maximum voltage applied was 5 V. As shown in Fig. 8a, TA2 substrates

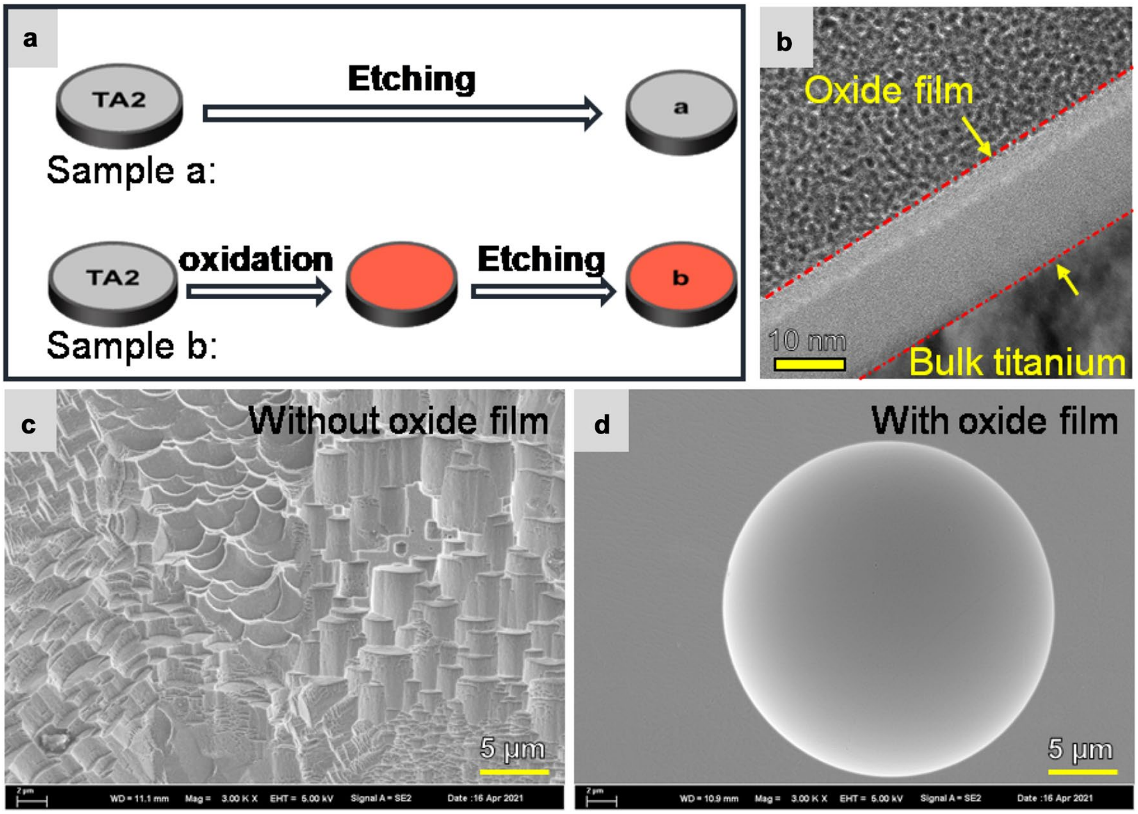

Fig. 7 **a** Schematic of sample preparation, **b** Cross section of the oxide film, and morphologies of TA2 substrates etched **c** without oxide film and **d** with an oxide film

were etched at different frequencies for 1 min in electrolyte with a 10:100 volume ratio of H_2SO_4:CH_3OH. The results showed that the root mean square of the current decreased with the increase in frequency. In turn, the increase in frequency reduced the duration of a single pulse, so the growth duration of the etching pits, the actual reaction area, and the current were all reduced. The current during etching at frequencies of 20 and 1000 Hz is shown in Fig. 8b. When the frequency was 20 Hz, the shape of the current followed the square wave. However, when the frequency was 1000 Hz, a peak was formed in the current, indicating the local charging of the double layers of the sample surface [43].

The surface morphology after etching at different frequencies is shown in Fig. 9. The results showed that the etching isotropy changed with frequency. When the frequency was 1, 10, and 20 Hz, the shape of the etching pits was irregular. When the frequency was 1 Hz, the etching pits were similar in shape and consisted of a relatively smooth area in the center surrounded by a relatively rough etching step area. These characteristics differed from those of the regularly shaped anisotropic etching pits in Fig. 4c. Every single pulse will cause the surface to be broken down again, and the breakdown site is usually on the edge of etching pits formed by the previous pulse [42]. As a result, the etching pits had irregular shapes, as shown in Fig. 9a. When the frequency was 10 Hz, the shape of the etching pits was similar to that of the hexagonal close-packed (hcp) structure with rough sides and placed at different angles, as shown in Fig. 9b. The rough sides were caused by the repeated breakdown and re-formation of the etching pits under pulsed power. In addition, the hcp structure indicated that the etching was anisotropic. This result can be explained as the increase in etching sites under the action of pulsed power, leading to an increase in the cross-sectional area of the mass transfer channel. As a consequence, electron transfer became the rate-determining step, resulting in anisotropic etching. When the frequency was 20 Hz, the morphology of the etching pit was similar to that obtained at 10 Hz. Given that the growth duration of the etching pit is short at 20 Hz, the size of the pit was smaller than that obtained at 10 Hz, as shown in Fig. 9c. When the frequency was increased to 50, 100, and 1000 Hz, hemispherical etching pits were distributed on the substrates, as shown

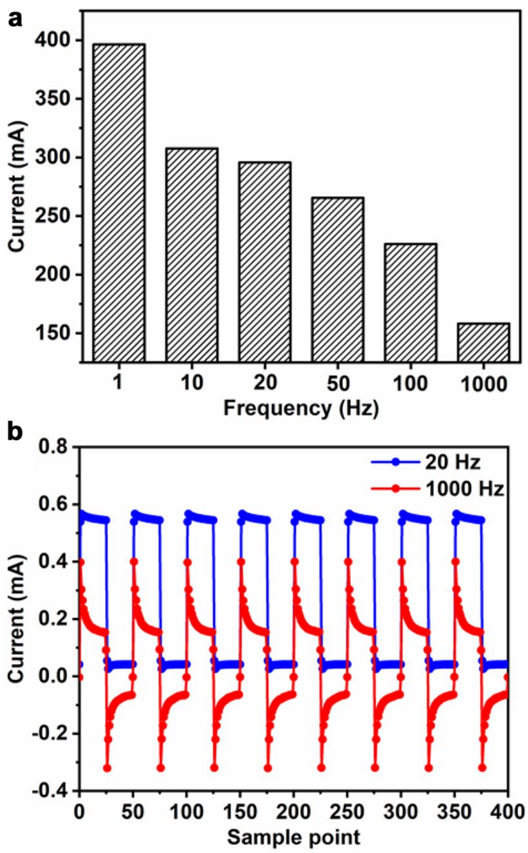

Fig. 8 **a** Effective current versus frequency and **b** current plots obtained at frequencies of 20 Hz and 1000 Hz

in Figs. 9d–f. When the frequency was further increased, the corresponding single pulse duration decreased, resulting in a reduction in the etching pit area. Therefore, the etching was isotropic due to the presence of few mass transfer channels. Meanwhile, the density of etching pits at the frequency of 1000 Hz was higher than that at the other two frequencies due to the higher breakdown frequency.

The application of pulsed power demonstrated that low frequencies such as 1, 10, and 20 Hz increased the etching sites. Hence, mass transfer was induced, rendering the etching to be charge transfer polarization. Pulse voltage with relatively low frequencies should be avoided to realize isotropic etching.

4.5 Tuning the etching isotropy of various metals

The electrochemical etching of common metals such as pure nickel, stainless steel 304, and aluminum alloy 6063 was carried out with a constant current of 0.5 A and a duration of 30 s to prove that mass transfer polarization is a generic approach for tuning the etching isotropy of metals. H_2SO_4 concentration was selected as the decisive variable for tuning the etching isotropy, although other variables have the same effect. When pure nickel was electrochemically etched in the electrolyte with an H_2SO_4:CH_3OH volume ratio of 1:100, anisotropic etch pits were formed, as shown in Fig. 10a1. When the H_2SO_4:CH_3OH volume ratio was increased to 20:100, isotropic etching sites were randomly distributed. For stainless steel 304, the shape of the etching pits changed from anisotropic to isotropic when the H_2SO_4:CH_3OH

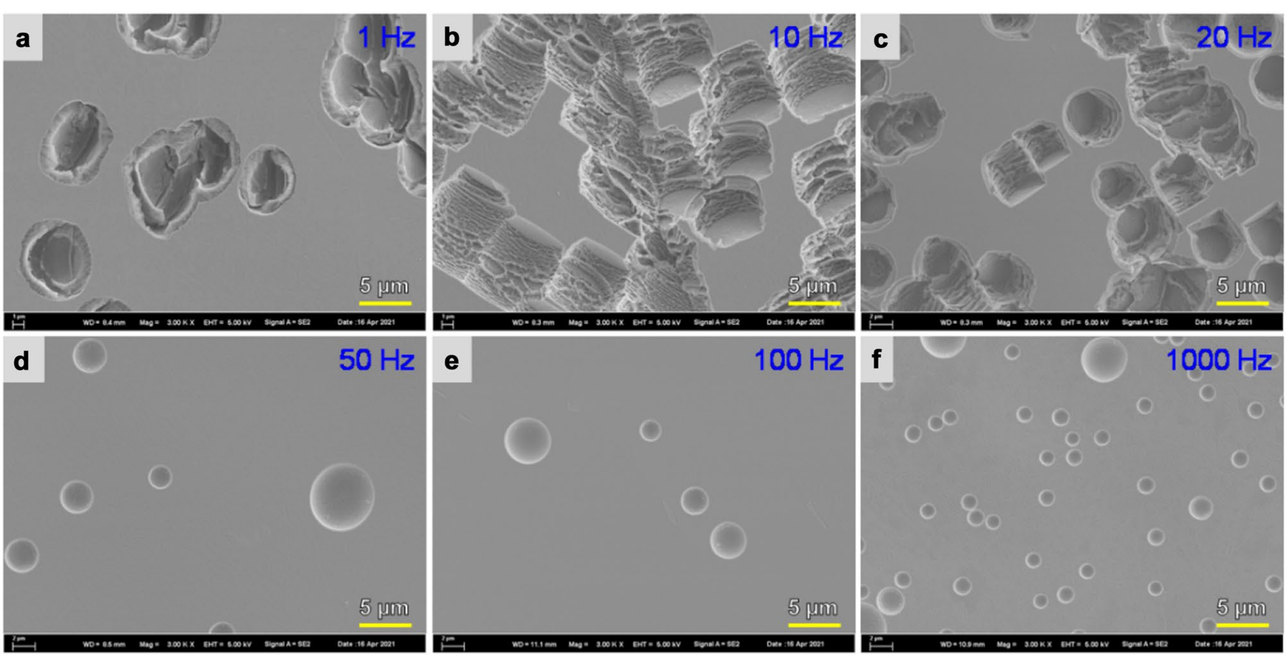

Fig. 9 Morphologies of the TA2 substrates etched at different frequencies: **a** 1, **b** 10, **c** 20, **d** 50, **e** 100, and **f** 1000 Hz

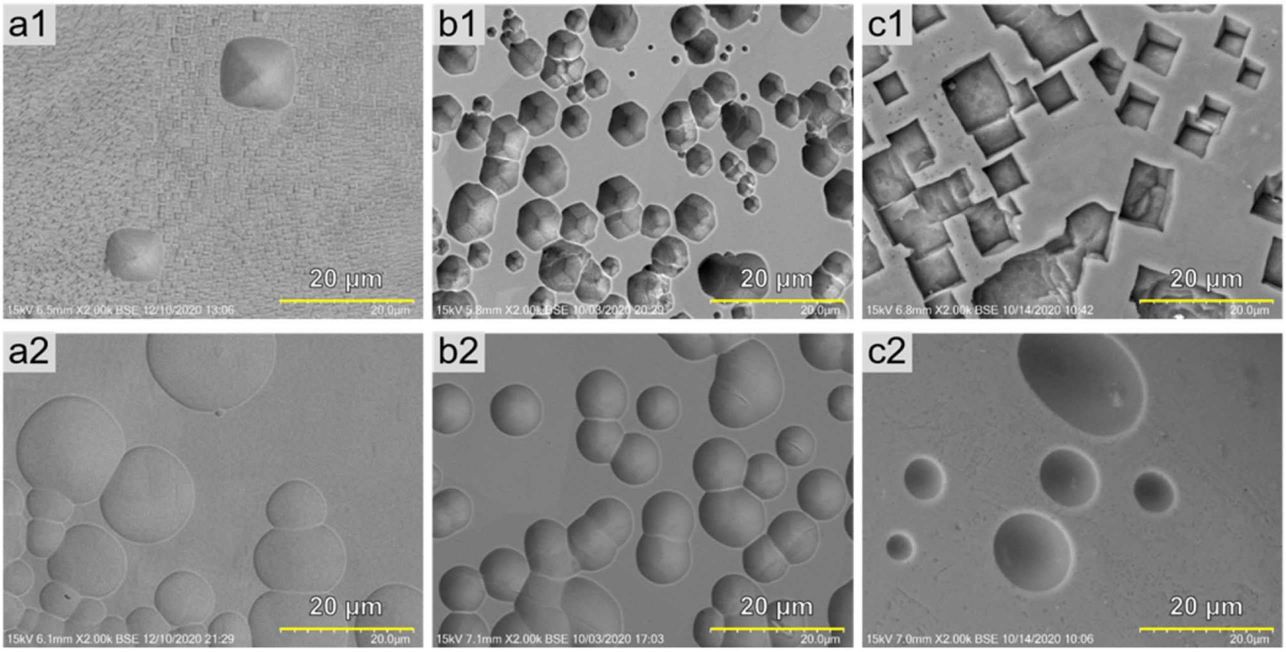

Fig. 10 SEM images of anisotropic and isotropic etch pits of some typical metals: **a1**, **a2** pure nickel, **b1**, **b2** stainless steel 304, and **c1**, **c2** aluminum alloy 6063

volume ratio of the electrolyte increased from 1:100 to 10:100, as shown in Figs. 10b1 and b2. For aluminum alloy 6063, cube-like etch pits were randomly distributed on the surface when the H_2SO_4:CH_3OH volume ratio of the electrolyte was 1:100, as shown in Fig. 10c1. Hemispheric etch pits were obtained in the electrolyte with an H_2SO_4:CH_3OH volume ratio of 30:100, as shown in Fig. 10c2.

As shown in Fig. 10, the etching isotropy was tuned by changing the H_2SO_4 concentration in the electrolyte for different metals. For isotropic etching, the shape of the etching pits was hemispheric, and the inner surface was smooth. In isotropic etching mode, the dissolution of metal depended on mass transfer and was not related to the characteristics of the crystal plane. Hence, the etching pits were hemispherical even for different metals, as shown in Fig. 10a2, b2, c2. However, for anisotropic etching, the shapes of the etch pits were complex due to differences in the atomic arrangement of different crystal planes. In addition, the lattice parameters of pure nickel, stainless steel 304, and 6063 aluminum alloy differ from each other; thus, the shape of the formed anisotropic etching holes also differed from each other, as shown in Fig. 10a1, b1, c1.

5 IEP of Metals

Given the feasibility of tuning the etching isotropy of various metals, the metals could be finished under isotropic etching conditions. TA2 was etched with a duration of 3 min and a current of 1.5 A under anisotropic (H_2SO_4:CH_3OH = 1:100) and isotropic (H_2SO_4:CH_3OH = 10:100) etch conditions. The SWLI images, profile, and SEM images of the TA2 surface are shown in Fig. 11. As shown in Fig. 11a1, a2, scratches and plowing marks were formed on the as-lapped surface. When the lapped surface was etched under the anisotropic mode, grains with different orientations exhibited different etch behaviors. The irregular etch pits merged together, and the surface was still rough, as shown in Fig. 11b1, b2. By contrast, the roughness was drastically reduced to 3.98 nm under isotropic etching, demonstrating the nanometric finishing capability of IEP, as shown in Fig. 11c1, c2. In addition, the material removal rate (MRR) of the IEP of TA2 was calculated by measuring the weight change before and after polishing. A high MRR of 11.7 μm/min was achieved, indicating that IEP is highly efficient for metal surface finishing.

The surface finishing of other metals and alloys under isotropic etching conditions was also conducted using the same electrolyte system of H_2SO_4 in CH_3OH. The finishing results of pure nickel, stainless steel 304, and aluminum alloy 6063 have been presented in our previous work [12]. Some metals and alloys that are difficult to polish by conventional energy beam polishing or ECP, including high melting point metal (pure tungsten), shape memory alloy (NiTi), and medium-entropy alloy (CoCrNi), were processed by IEP to demonstrate the general applicability of IEP. Figure 12a–c shows that surfaces with nanoscale Sa roughness were obtained for all the tested materials that were originally processed by lapping. The optical photos after etching are shown in Fig. 12d, showing

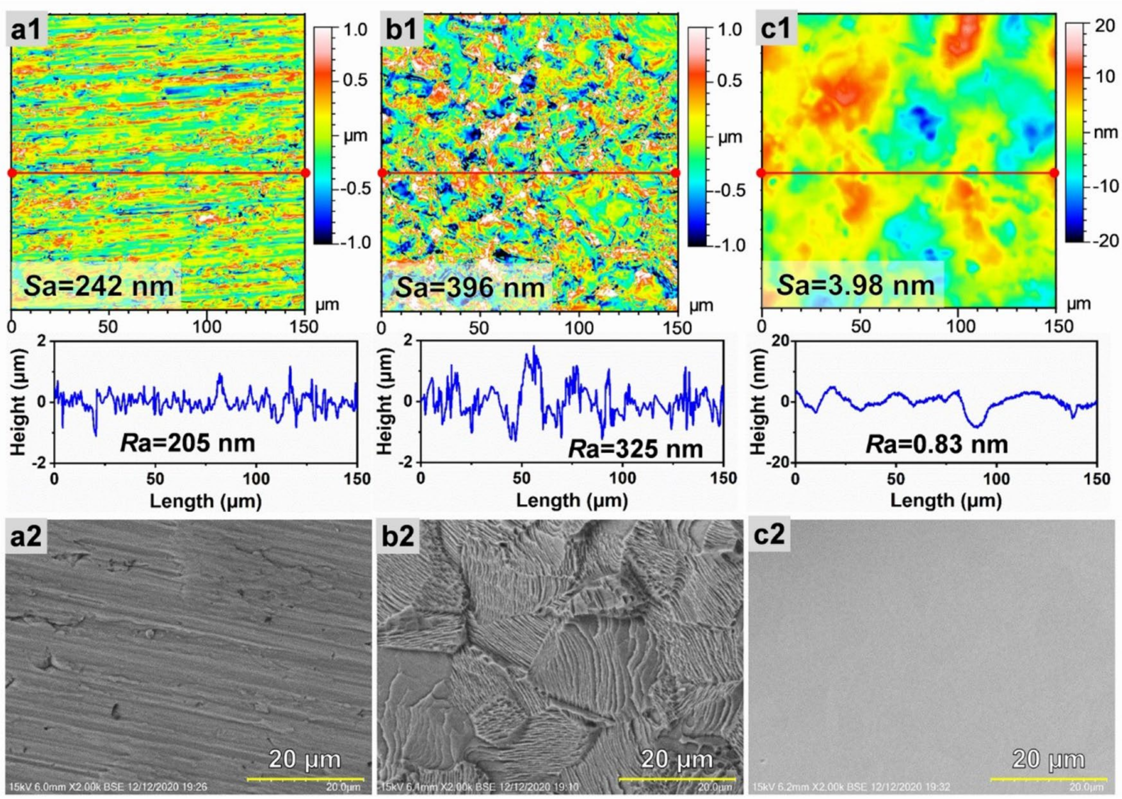

Fig. 11 SWLI (cut-off length: 25 μm) and SEM images of TA2 surfaces. **a1**, **a2**: original lapped surface; **b1**, **b2**: anisotropically etched surface; and **c1**, **c2**: isotropically etched surface

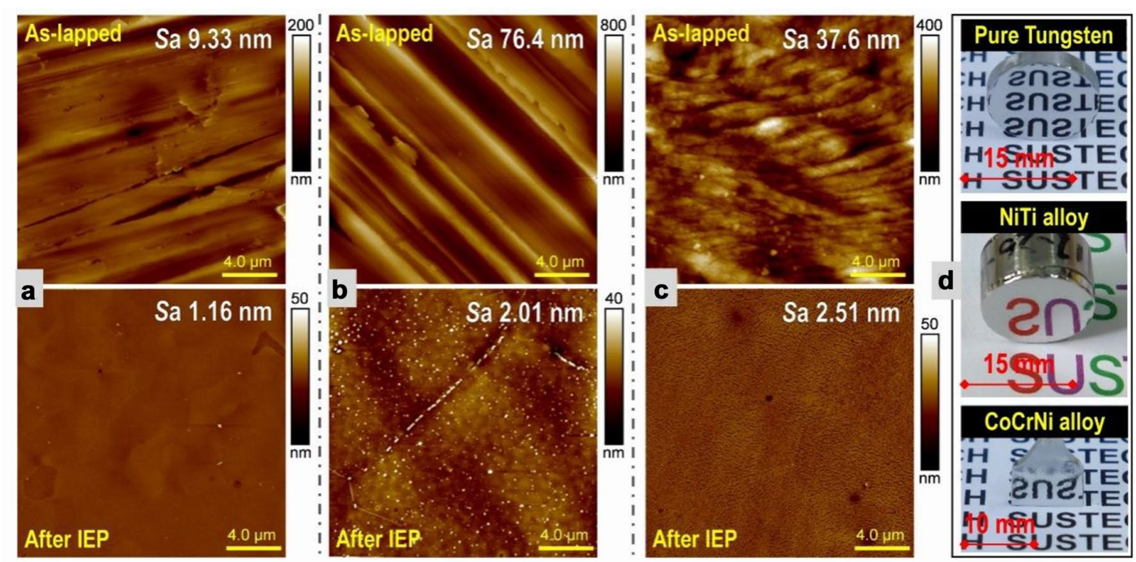

Fig. 12 AFM images of as-lapped and polished surfaces: **a** Pure tungsten (3 A, H_2SO_4:CH_3OH = 15:100, 1 min); **b** NiTi alloy (3 A, H_2SO_4:CH_3OH = 10:100, 1 min); and **c** CoCrNi (3 A, H_2SO_4:CH_3OH = 10:100, 1 min). **d** Photographs of the polished samples

that a mirror-like surface was obtained by IEP. The MRRs of the IEP of pure tungsten, NiTi alloy, and CoCrNi alloy were 13.3, 28.9, and 19.0 μm/min, respectively.

6 Conclusions and Outlook

IEP is a generic approach for metal surface finishing. In this work, the tuning of the etching isotropy of various metals was studied to elucidate the polishing mechanism of IEP. The conclusions were as follows:

(1) IEP is a sequential process that includes the following steps: passivation, breakdown of the passivation layer, and formation and merging of the etch pits.
(2) Mass transfer polarization is the key to realizing the isotropic etching of metals. The etching isotropy of various metals can be tuned by optimizing the etching conditions. The diffusion coefficient of the electrolyte, which can be controlled by H_2SO_4 and $C_3H_8O_3$ concentrations, is the most effective parameter for tuning the etching isotropy.
(3) Under the isotropic etching mode, various metals and alloys can be efficiently polished, and nanoscale Sa roughness has been achieved.

With this newly developed IEP technique, the surface finish of metals can be achieved down to the atomic scale. Hence, IEP is an effective candidate for atomic and close-to-atomic scale manufacturing [44].

Acknowledgements This project is supported by the National Natural Science Foundation of China (52035009, 52005243) and the Science and Technology Innovation Committee of Shenzhen Municipality (JCYJ20200109141003910, JCYJ20210324120402007, KQTD20170810110250357). The authors acknowledge the assistance of SUSTech Core Research Facilities.

Declarations

Conflict of interest The authors have no conflicts of interest to declare that are relevant to the content of this article.

References

1. Xiao G, Zhao H, Zou L, Zhao L, Liu Y, Dai W (2018) Residual stress of belt polishing for the micro-stiffener surface on the titanium alloys. Procedia CIRP 71:11–15
2. Tsai M-Y, Yang W-Z (2012) Combined ultrasonic vibration and chemical mechanical polishing of copper substrates. Int J Mach Tools Manuf 53:69–76
3. Evans CJ, Paul E, Dornfeld D, Lucca DA, Byrne G, Tricard M, Klocke F, Dambon O, Mullany BA (2003) Material removal mechanisms in lapping and polishing. CIRP Ann 52:611–633
4. Hashimoto F, Yamaguchi H, Krajnik P, Wegener K, Chaudhari R, Hoffmeister H-W, Kuster F (2016) Abrasive fine-finishing technology. CIRP Ann 65:597–620
5. Yuan F, Liu C, Gu H, Han F, Zhang Y, Ali M, Li G (2019) Effects of mechanical polishing treatments on high cycle fatigue behavior of Ti-6Al-2Sn-4Zr-2Mo alloy. Int J Fatigue 121:55–62
6. Pfefferkorn FE, Duffie NA, Li X, Vadali M, Ma C (2013) Improving surface finish in pulsed laser micro polishing using thermocapillary flow. CIRP Ann 62:203–206
7. Okada A, Uno Y, McGeough JA, Fujiwara K, Doi K, Uemura K, Sano S (2008) Surface finishing of stainless steels for orthopedic surgical tools by large-area electron beam irradiation. CIRP Ann 57:223–226
8. Deng T, Li J, Zheng Z (2020) Fundamental aspects and recent developments in metal surface polishing with energy beam irradiation. Int J Mach Tools Manuf. 148:103472
9. Han W, Fang F (2019) Fundamental aspects and recent developments in electropolishing. Int J Mach Tools Manuf 139:1–23
10. Kawanaka T, Kunieda M (2015) Mirror-like finishing by electrolyte jet machining. CIRP Ann 64:237–240
11. Wang F, Zhang X, Deng H (2019) A comprehensive study on electrochemical polishing of tungsten. Appl Surf Sci 475:587–597
12. Yi R, Zhang Y, Zhang X, Fang F, Deng H (2020) A generic approach of polishing metals via isotropic electrochemical etching. Int J Mach Tools Manuf. 150:103517
13. Matlosz M, Magaino S, Landolt D (1994) Impedance analysis of a model mechanism for acceptor-limited electropolishing. J Electrochem Soc 141:410–418
14. Grimm RD, West AC, Landolt D (1992) AC impedance study of anodically formed salt films on iron in chloride solution. J Electrochem Soc 139:1622–1629
15. Ma H, Chen X-Q, Li R, Wang S, Dong J, Ke W (2017) First-principles modeling of anisotropic anodic dissolution of metals and alloys in corrosive environments. Acta Mater 130:137–146
16. Yanagishita T, Imaizumi M, Kondo T, Masuda H (2017) Formation of porous Al particles by anisotropic anodic etching. Electrochem Commun 78:26–28
17. Fu B, Liu W, Li Z (2010) Surface energy calculation of alkali metals with the empirical electron surface model. Mater Chem Phys 123:658–665
18. Wang J, Wang S-Q (2014) Surface energy and work function of fcc and bcc crystals: Density functional study. Surf Sci 630:216–224
19. Jee SE, Lee PS, Yoon B-J, Jeong S-H, Lee K-H (2005) Fabrication of microstructures by wet etching of anodic aluminum oxide substrates. Chem Mater 17:4049–4052
20. Oh H-J, Lee J-H, Ahn H-J, Jeong Y, Park N-J, Kim S-S, Chi C-S (2007) Etching characteristics of high-purity aluminum in hydrochloric acid solutions. Mater Sci Eng, A 449–451:348–351
21. Bard A, Faulkner L (2002) Electrochemical methods: fundamentals and applications. John Wiley & Sons Inc, New York

22. Landolt D, Chauvy PF, Zinger O (2003) Electrochemical micromachining, polishing and surface structuring of metals: Fundamental aspects and new developments. Electrochim Acta 48:3185–3201
23. Matlosz M (1995) Modeling of impedance mechanisms in electropolishing. Electrochim Acta 40:393–401
24. Wang D, Zhu Z, He B, Ge Y, Zhu D (2017) Effect of the breakdown time of a passive film on the electrochemical machining of rotating cylindrical electrode in $NaNO_3$ solution. J Mater Process Technol 239:251–257
25. Yang G, Wang B, Tawfiq K, Wei H, Zhou S, Chen G (2016) Electropolishing of surfaces: theory and applications. Surf Eng 33:149–166
26. Reggiani RC, Mazza F, Sivieri E (1979) Electrochemical polishing of titanium in perchloric-methanolic solutions. Mater Chem 4:149–158
27. Piotrowski O, Madore C, LandoIt D (1998) The mechanism of electropolishing of titanium in methanol-sulfuric acid electrolytes. J Electrochem Soc 145:2362–2369
28. Smialowska ZS (1971) Review of literature on pitting corrosion published since 1960. Corros Eng 27:223–233
29. Mato S, Alcalá G, Woodcock TG, Gebert A, Eckert J, Schultz L (2005) Corrosion behaviour of a Ti-base nanostructure-dendrite composite. Electrochim Acta 50:2461–2467
30. Ittah R, Amsellem E, Itzhak D (2014) Pitting corrosion evaluation of titanium in NH4Br solutions by electrochemical methods. Int J Electrochem Sci 9:633–643
31. Alves VA, Reis RQ, Santos ICB, Souza DG, de F. Gonçalves T, Pereira-da-Silva MA, Rossi A, da Silva LA (2009) In situ impedance spectroscopy study of the electrochemical corrosion of Ti and Ti–6Al–4V in simulated body fluid at 25 °C and 37 °C. Corrosion Sci, 51:2473–2482
32. Izquierdo J, González-Marrero MB, Bozorg M, Fernández-Pérez BM, Vasconcelos HC, Santana JJ, Souto RM (2016) Multiscale electrochemical analysis of the corrosion of titanium and nitinol for implant applications. Electrochim Acta 203:366–378
33. Punkkinen MPJ, Hu QM, Kwon SK, Johansson B, Kollár J, Vitos L (2011) Surface properties of 3D transition metals. Phil Mag 91:3627–3640
34. Fushimi K, Kondo H, Konno H (2009) Anodic dissolution of titanium in chloride-containing ethylene glycol solution. Electrochim Acta 55:258–264
35. Wang Y, Xu Z, Zhang A (2019) Electrochemical dissolution behavior of Ti-45Al-2Mn-2Nb+0.8 vol% TiB2 XD alloy in NaCl and NaNO3 solutions. Corros Sci 157:357–369
36. Liu W, Ao S, Li Y, Liu Z, Zhang H, Manladan SM, Luo Z, Wang Z (2017) Effect of anodic behavior on electrochemical machining of TB6 titanium alloy. Electrochim Acta 233:190–200
37. Bolat G, Izquierdo J, Santana JJ, Mareci D, Souto RM (2013) Electrochemical characterization of ZrTi alloys for biomedical applications. Electrochimica Acta 88:447–456
38. He Y, Lu W, Gan W, Zhao J, Zuo D (2016) Polarization of Ti6Al4V alloy in NaBr electrolyte and surface fractal analysis. Proc Inst Mech Eng Part L J Mater Des Appl 232:602–609
39. Li T, Swanson OJ, Frankel GS, Gerard AY, Lu P, Saal JE, Scully JR (2019) Localized corrosion behavior of a single-phase non-equimolar high entropy alloy. Electrochim Acta 306:71–84
40. Fushimi K, Neelakantan L, Eggeler G, Hassel AW (2018) On the electropolishing mechanism of nickel titanium in methanolic sulfuric acid − an electrochemical impedance study. Phys Status Solidi (a) 215:1800011
41. Wang L, Yu H, Wang K, Xu H, Wang S, Sun D (2016) Local Fine structural insight into mechanism of electrochemical passivation of titanium. ACS Appl Mater Interf 8:18608–18619
42. Dyer CK, Alwitt RS (1981) Surface changes during A.C. etching of aluminum. J Electrochem Soc 128:300–305
43. Rolf S, Viola K, Philippe A, Gerhard E (2000) Electrochemical micromachining. Science 289:98–101
44. Mathew PT, Rodriguez BJ, Fang F (2020) Atomic and close-to-atomic scale manufacturing: a review on atomic layer removal methods using atomic force microscopy. Nanomanuf Metrol 3:167–186